chemosensors

MDPI

Article

Novel 1D/2D KWO/$Ti_3C_2T_x$ Nanocomposite-Based Acetone Sensor for Diabetes Prevention and Monitoring

Obinna Ama [1,†], Mahek Sadiq [1,†], Michael Johnson [2], Qifeng Zhang [1,2,3] and Danling Wang [1,2,3,*]

[1] Biomedical Engineering Program, North Dakota State University, Fargo, ND 58102, USA; obinna.ama@ndsu.edu (O.A.); mahek.sadiq@ndsu.edu (M.S.); qifeng.zhang@ndsu.edu (Q.Z.)
[2] Materials and Nanotechnology Program, North Dakota State University, Fargo, ND 58102, USA; michael.johnson.1@ndsu.edu
[3] Department of Electrical and Computer Engineering, North Dakota State University, Fargo, ND 58102, USA
* Correspondence: danling.wang@ndsu.edu; Tel.: +1-701-231-8396
† These authors contributed equally to this work.

Received: 30 August 2020; Accepted: 14 October 2020; Published: 16 October 2020

Abstract: The acetone content in the exhaled breath of individuals as a biomarker of diabetes has become widely studied as a non-invasive means of quantifying blood glucose levels. This calls for development of sensors for the quantitative analysis of trace concentration of acetone, which is presents in the human exhaled breath. Traditional gas detection systems, such as the Gas Chromatography/Mass Spectrometry and several types of chemiresistive sensors are currently being used for this purpose. However, these systems are known to have limitations of size, cost, response time, operating conditions, and consistent accuracy. An ideal breath acetone sensor should provide solutions to overcome the above limitations and provide good stability and reliability. It should be a simple and portable detection system of good sensitivity, selectivity that is low in terms of both cost and power consumption. To achieve this goal, in this paper, we report a new sensing nanomaterial made by nanocomposite, 1D KWO ($K_2W_7O_{22}$) nanorods/2D $Ti_3C_2T_x$ nanosheets, as the key component to design an acetone sensor. The preliminary result exhibits that the new nanocomposite has an improved response to acetone, with 10 times higher sensitivity comparing to KWO-based sensor, much better tolerance of humidity interference and enhanced stability for multiple months. By comparing with other nanomaterials: Ti_3C_2, KWO, and KWO/$Ti_3C_2T_x$ nanocomposites with variable ratio of KWO and $Ti_3C_2T_x$ from 1:1, 1:2, 1:5, 2:1, 4:1, and 9:1, the initial results confirm the potential of the novel KWO/Ti_3C_2 (2:1) nanocomposite to be an excellent sensing material for application in sensitive and selective detection of breath acetone for diabetics health care and prevention.

Keywords: KWO/$Ti_3C_2T_x$ nanocomposite; chemiresistive response; diabetes; breath acetone

1. Introduction

The number of people living with diabetes in the world has continued to increase, with nearly 463 million adults between ages 20–79, as reported by the International Diabetes Federation (IDF) [1]. Future projections estimate this number can be increased to about 700 million people by 2045 [1]. This means that if urgent actions are not taken, diabetes will become a global health emergency to impact on mortality rates and economic productivity. Frequent monitoring of blood glucose levels is a crucial step in the management of diabetes and extensively prevents exacerbation of the disease. In recent years, a variety of apparatuses based on blood glucose measurement have been introduced into practice (i.e., blood sensors and urinalysis), although some are still under their developing stages, such as breath-based sensors.

Studies indicate that the blood glucose level is closely related to the concentration of acetone in exhaled breath [2]. Breath acetone or dimethyl ketone is a volatile organic compound and known for its rotten apple smell, as described by physicians [3], which is physiologically produced in the body as one of the three by-products of ketoacidosis—when the liver breaks down fats to produce energy in response to the body's inability to utilize glucose [3,4]. Given this reason, elevated level of acetone in the exhaled breath can be used as the biomarker to diagnose diabetes. Generally, the concentration of breath acetone levels for healthy person is between 0.4 ppm (parts-per-million) to 0.9 ppm while 1.8 ppm and above for diabetics [5]. Individuals with acetone levels between 0.9 and 1.8 are considered to be at risk of developing diabetes in the future [5–7]. This paper reports a new portable sensor device based a novel sensing nanomaterial, KWO/$Ti_3C_2T_x$ nanocomposites, for sensitive and selective detection of trace concentration acetone, as a potential simple, low-cost, portable, non-invasive, and user-friendly tool to help diabetics monitoring their daily health condition and preventing the complications caused by this disease.

Several techniques have been developed to determine acetone concentration in exhaled breath. One of the conventional methods used for quantifying breath acetone is Gas Chromatograph (GC) paired with a Flame Ion Detection (FID) or Mass Spectrometry (MS) incorporated [8,9]. Such techniques can provide accurate measurements of breath acetone but are bulky, heavy, expensive, complicated, and time-consuming [10]. Real-time detection of acetone in exhaled breath has been made possible with the use of proton transfer reaction-mass spectrometry (PTR-MS) and the selected ion flow-mass spectrometry (SIFT-MS). However, they are still costly, bulky and require frequent calibration [11]. In order to overcome above limitations associated with size, cost, and complexity of these quantitative analytical techniques, researchers started to investigate new sensing techniques by using metal oxide semiconductors (MOS) to detect breath acetone. In particular, the nanostructured MOS-based chemiresistive sensors are now widely used for gas sensors due to their attractive electrical and material properties which enable detection of target gases [12–22] with enhanced sensitivity, fast response, low cost and capability of miniaturization. The sensing mechanism of chemiresistive response works by changing resistance of the sensing material in response to surface adsorption and desorption of gas molecules. This interaction leads to the formation of an electron-depleted region. That is, the gas detection in semiconductor-based sensors is related to ionosorbed surface oxygen and target analyte gas that causes a change in the conductivity of the semiconductor materials [23,24]. Table 1 lists current MOS-based chemiresistive sensors which have been reported to detect acetone. These semiconductors include Tungsten (VI) oxide (WO_3), Tin(IV) Oxide (SnO_2), Zinc oxide (ZnO), Titanium dioxide (TiO_2), Iron (III) oxide(Fe_2O_3), Indium (III) oxide (In_2O_3), Copper (II) oxide (CuO), ZnO-CuO, and KWO (our work) [13–22].

The performance of these sensing materials can be improved either through modification of sensor device configuration/structure or combination with other nanomaterials to form nanocomposites in order to facilitate interaction with gas acetone molecules. For example, ZnO-CuO core-hollow cube nanostructures-based *p-n* heterojunction chemiresistive sensor exhibits a remarkable response to acetone at 200 °C. The lowest concentration can be detected down to 0.04 ppm with high selectivity and excellent stability for up to 40 days [13]. However, all these sensors are operating at an elevated temperature at least (200 °C), which ultimately increase the power requirements and overall cost of the devices. In contrast, the as-synthesized $K_2W_7O_{22}$ (KWO), a new functionalized semiconductor nanomaterial in our group, has been validated to be able to operate at room temperature with sensitive and selective response to acetone [22]. This is because KWO-based sensing mechanism is different than traditional MOS-based chemiresistive sensors, due to its unique material and surface properties. Detailed discussion of KWO sensing acetone can be found somewhere else [22,25–30]. The brief summary in this paper focuses on the *p*-type semiconductor property, high surface area and porous morphology, and specifically the room-temperature ferroelectric property. All these structural and material properties enable nanostructured KWO to effectively interact with the high dipole-moment compound, acetone, thereby causing a significant change of the resistance [22,25–30]. However, the results indicate that water vapor can cause a strong interference and baseline shift to weaken KWO

sensing performance [30]. We need to find a solution which can effectively address the water vapor interference and baseline shift in KWO-based sensors.

Table 1. Selected Metal Oxide Semiconductors as acetone sensor.

Material	Principle of Operation Device Type	Lowest Concentration Detected (ppm)	Response Time	Operation Temperature
ZnO-CuO [13]	Resistance change Core-hollow cube	0.04 ppm	5.59 s for 0.5 ppm	200 °C
In_2O_3 [14]	Resistance change Nanowire	25 ppm	~10 s (in N_2)	400 °C
InN [15]	Resistance change Thin Films	0.4 ppm	150 s for 10 ppm (in air)	200 °C
GaN [16]	Resistance change thin Films	500 ppm	10 s for 1000 ppm (in air)	350 °C
WO_3 [16]	Resistance change Nanoparticles	0.2 ppm	~3.5 m	400 °C
WO_3 Fibers w/Pt [17]	Resistance change Nanoparticles	0.12 ppm	5 min (in air)	300 °C
In/WO_3-SnO_2 [18]	Resistance change thin films	Verify	Verify	200 °C
ZnO [19]	Resistance change thin film	100 ppm	30 s	200 °C
Fe_2O_3 [20]	Resistance change Thin Film	500 ppm	33 s (in air)	275 °C
TiO_2 [21]	Resistance change Thin Film	1 ppm	10 s (in air)	500 °C
$K_2W_7O_{22}$ [22]	Resistance change Thin Film	0.5 ppm	~30 s *	25 °C

* our work.

Currently, our group has successfully synthesized a new 2-dimentional (2D) nanomaterial, $Ti_3C_2T_x$ (T_x stands for OH^-, –O, and F^{-1} surface terminated groups). MXene, named from the general formula of $M_{n+1}X_n$ (n = 2, M = Ti, and X = C) [31,32]. Due to the unique multi-layered structure with extreme large surface and interface area, metallic conductivity, and flexible surface functionality, 2D MXene $Ti_3C_2T_x$, attracts a lot of attention in the field of biomedical sensing and energy storage with high signal to noise ratio [31–37]. Motivated by these findings, here, we aim to explore the potential of using 1D KWO and 2D $Ti_3C_2T_x$ nanocomposite as the new sensing material for acetone detection which is low cost, highly sensitive and selective, low noise, low interference from water vapor, and room-temperature operation. The details are described below.

2. Experiments

2.1. Material Synthesis

The KWO sensor nanomaterial was synthesized using the hydrothermal method which has been described in our previous report [22]. Briefly, a precursor solution containing $Na_2WO_4{\cdot}2H_2O$ (95%, Alfa Aesar, Haverhill, MA, USA), oxalic acid dihydrate (>99%, VWR, Radnor, PA, USA), K_2SO_4 (>99%, VWR, Radnor, PA, USA) and HCl (36%–38%, Aqua Solutions Inc. Deer Park, TX, USA) was made. This solution was then put into a 30 ml autoclave for synthesis. KWO samples were grown at 225 °C for 24 h. Sensor materials used for acetone sensing tests were made by blade coating and then annealed at 350 °C. X-ray diffraction (XRD) was obtained using a Bruker AXS D8 Discover to study as-synthesized

KWO crystalline structure (Bruker, Billerica, MA, USA). Sensors were prepared by coating a paste made from KWO and ethanol on glass substrates. A diffraction pattern was gathered from a 2-Theta of 5° to 90°. Scanning electron microscopy (SEM) image was obtained using a JEOL JEM-2100 high-resolution analytical TEM (JEOL Ltd., Tokyo, Japan).

Pure $Ti_3C_2T_x$ MXene was synthesized based on an Hydrofluoric (HF) etching method [38,39]. Our group has recently developed a "hot etching" method which can make high-yield, high purity of $Ti_3C_2T_x$ MXene [40]. In detail, 1) a precursor, so-called Ti_3AlC_2 MAX phase was synthesized by first ball milling TiC, Ti, and Al powders for 5 h. The TiC:Ti:Al molar ratio was 2:1:1.2, respectively. Excess Al powder was used due to reporting of an Al deficiency even when used in proper molar ratio due to unknown reasons. The resulting powder is then pressed into a pellet and sintered at 1350 °C for 4 h under argon flow. The collected pellet is then milled back into powder and sieved through a 160-mesh sieve. The MAX powder was then collected and used in the high temperature etching experiments. A total of 0.5 g of MAX phase was etched using HF acid in a 25 ml Teflon lined autoclave at temperature of 150 °C for five hours in a Thermolyne furnace. HF concentration of 5%wt was used to remove Al-layers from the MAX phase. Materials were then sonicated for 1 hour using a sonicating bath and collected via centrifuge. All materials were then dried overnight at 65 °C in a drying oven.

The nanocomposite film made by KWO and $Ti_3C_2T_x$ MXene was formed with variable material ratios of KWO/$Ti_3C_2T_x$–1:1, 1:2, 1:5, 2:1, 4:1, and 9:1 using electrostatic self-assembly technique. In detail, amounts of as-synthesized KWO nanorods were dispersed into distilled water and sonicated for 1h. Then, 10mg of as-synthesized $Ti_3C_2T_x$ nanosheets were added to 10 mL distilled water and sonicated for 1h. Thereafter, the homogeneous KWO solution was poured into the $Ti_3C_2T_x$ solution. After that, the mixture was stirred vigorously for 12 h. Finally, the obtained KWO/$Ti_3C_2T_x$powder was washed three times with distilled water and dried at 80 °C for 24 h [41]; Finally, eight as-synthesized nanomaterials including $Ti_3C_2T_x$, KWO, and KWO/$Ti_3C_2T_x$ (1:1, 1:2, 1:5, 2:1, 4:1, and 9:1) were made into thin films using drop-casting method on the gold-electrode patterned glass substrates.

2.2. Sensing Test System

For a typical chemiresistive device, the sensitivity, as described in equation (1), is calculated about the resistance change once the sensing film exposed to the analyte gas. A couple of factors have previously been reported on KWO sensing acetone to significantly influence device performance, such as the shift of baseline resistance of the film and interference of relative humidity (RH) [22,26,30]. Hence, the sensing system for this study, was focusing on how to improve the performance of as-reported acetone sensor with less interference of humidity and long-term stability.

The acetone vapor and RH can be generated and controlled through an OVG-4 vapor generator and humidity generator, OHG-4 (Owlstone Inc., Westport, CT, USA), as shown in Figure 1. The vapor generator was designed to generate trace concentrations of gases precisely. For example, using OVG-4 vapor generator, we can obtain variable concentrations of acetone vapor ranging from 0.1 ppm to 5.6 ppm with controlled RH levels from 8% up to 85%. The sensing test has been conducted to detect variable concentration of acetone at a certain RH under the room temperature. The change in resistance across the film was measured using the Keithly electrometer. RH and temperature were monitored using a commercialized sensor. The concentrations of acetone vapor used in this study is 2.85 ppm with 10%, 50% and 70% RH conditions, respectively, at the room temperature. To conduct the experiment, baseline resistance of the sensors at room RH (between 20%–40%) was measured and recorded, as R1. The generated acetone and water vapor are delivered through carrier gas from OVG-4 and OHG into the sensing chamber.

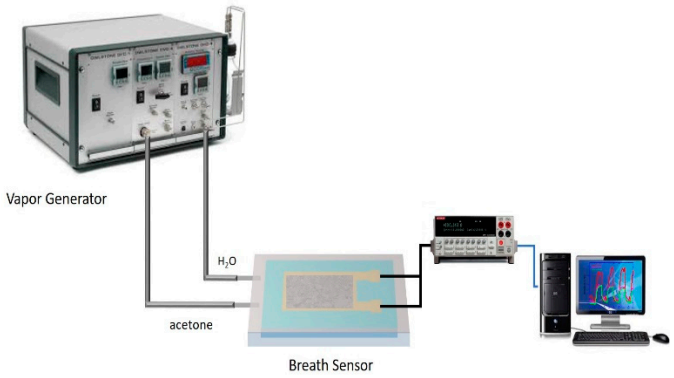

Figure 1. Diagram showing the acetone testing system. Acetone and humidity are generated by the Owlstone vapor and humidity generator and delivered into the sensor testing box.

The sensitivity of the sensor films to acetone at a given RH value can be calculated as the percentage change in resistance of the sensing material with and without exposure of acetone:

$$S\% = \left(\frac{R3 - R2}{R1}\right) \times 100 \quad (1)$$

Here, S is sensitivity (%) to acetone, $R1$ is the baseline resistance (MΩ) at room RH, $R2$ is the resistance (MΩ) at the controlled RH without acetone in-flow and $R3$ is the resistance (MΩ) at the same controlled RH with acetone in-flow.

3. Results and Discussion

3.1. Characterization

The microstructures and morphologies of the as-synthesized nanomaterials: KWO, $Ti_3C_2T_x$, KWO/$Ti_3C_2T_x$ nanocomposites have been investigated by SEM. As shown in Figure 2a, the SEM image of KWO clearly shows a three-dimensional mesh of randomly orientated and interconnected nanorods with several μm in length and 20–50 nm in diameter. The SEM image of pristine $Ti_3C_2T_x$ MXene (Figure 2b) exhibits multilayered structure and accordion-like morphology. Figure 2c–f show the SEM images of the KWO/$Ti_3C_2T_x$ nanocomposites at the ratio 2:1, 1:1, 4:1, and 9:1, which all indicate a rougher surface due to the decoration of the KWO nanorods on the $Ti_3C_2T_x$ nanosheets and illustrate the successful construction of the 1D/2D KWO/$Ti_3C_2T_x$ hybrids. This could suggest a strongly coupled interaction between KWO and $Ti_3C_2T_x$.

The XRD patterns of the as-synthesized samples (KWO, $Ti_3C_2T_x$ MXene, and KWO/$Ti_3C_2T_x$ nanocomposites) are shown in Figure 3. The peak at $2\theta = 6.2°$ is corresponding to the (002) facet of $Ti_3C_2T_x$. While the peaks at $2\theta = 23°, 28°$ correspond to (002) and (200) of KWO. In our previous reports [22–24], the relative peaks (002)/(200) play an important role to realize the selective detection of acetone. The XRD spectrum of KWO/$Ti_3C_2T_x$ (2:1) nanocomposite has shown the strongest relative peak at (002). In addition, nanocomposites show higher crystalline structure while the ratio of KWO/$Ti_3C_2T_x$ is higher. Beside these, the much weaker intensity of MXene observed in XRD indicates that the content of the $Ti_3C_2T_x$ in the composite is very low. The low content of $Ti_3C_2T_x$ in the nanocomposites means $Ti_3C_2T_x$ will not cause dramatic change of material properties, e.g., *p*-type semiconducting, and ferroelectricity, but KWO has interacted with $Ti_3C_2T_x$ in the nanocomposites and caused the change of their crystal facets.

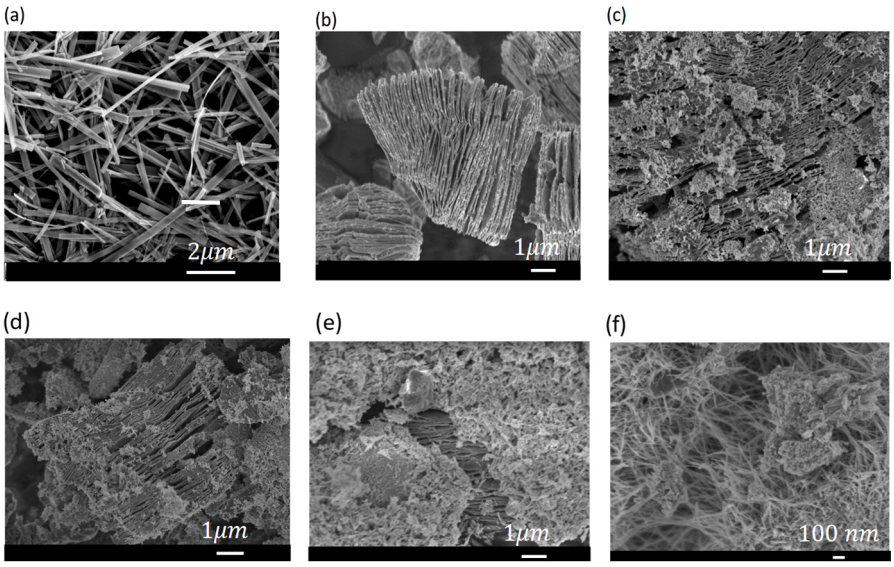

Figure 2. SEM images of (**a**) KWO nanorods, (**b**) $Ti_3C_2T_x$, (**c**) KWO/$Ti_3C_2T_x$ (2:1), (**d**) KWO/$Ti_3C_2T_x$ (1:1), (**e**) KWO/$Ti_3C_2T_x$ (4:1), and (**f**) KWO/Ti_3C_{2x} (9:1).

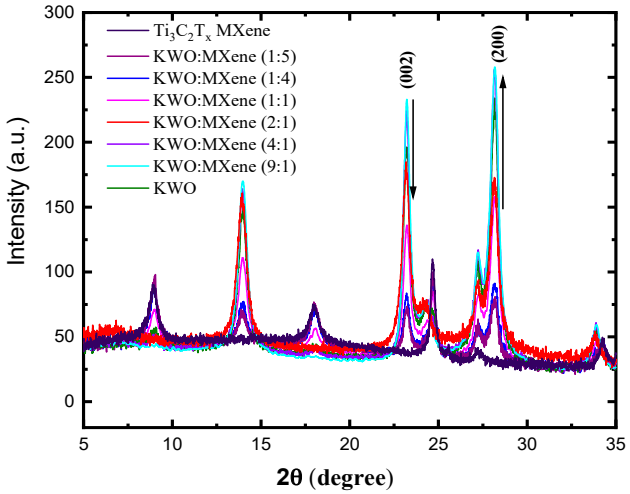

Figure 3. XRD spectra of KWO nanorods, $Ti_3C_2T_x$MXene, and KWO/$Ti_3C_2T_x$ nanocomposites, and $Ti_3C_2T_x$ MXene.

3.2. Sensing Tests

The sensing performance of as-fabricated device to detect acetone is based on a room-temperature chemiresistive response. That is, the detection and sensing response of acetone largely depend on sensing material's chemical, electrical and structural properties. These properties play an important role to affect charge transfer between sensing material and detected gas, and electrons/holes diffusion within the nanocomposite. This results in a change in resistance of sensing material [38,39]. As shown in Figure 4, comparing to other nanomaterials, the KWO/$Ti_3C_2T_x$ (2:1) nanocomposite exhibits the highest sensitivity (almost 10 times higher than the response of KWO) to 2.86 ppm acetone at the same sensing condition, RH = 20% and room temperature. Although the detailed sensing mechanism is still under investigation, the improved sensing performance of KWO/$Ti_3C_2T_x$ (2:1) nanocomposite can be considered due to the contributions of (1) the unique surface and electric properties of $Ti_3C_2T_x$ nanosheets [38,42], which can provide better signal to noise ratio and higher sensitivity, (2) the room temperature of ferroelectric property of KWO [22], and (3) the interaction between KWO and $Ti_3C_2T_x$ makes stronger (002) facet. Here, 2D multilayered $Ti_3C_2T_x$ nanosheets not only provide extreme large

surface and interface area for the absorption of acetone molecules but also the rich surface functional groups, T_x (–O, –OH, and –F). These can be the active sites for the nucleation and growth of the KWO nanorods to enhance the interfacial interactions between KWO and $Ti_3C_2T_x$ and expedite charge transfer and transportation.

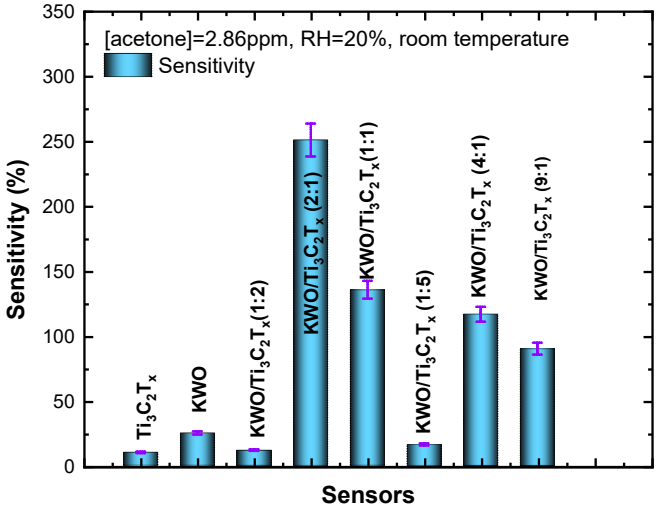

Figure 4. Sensing test on 2.86 ppm acetone at room temperature, RH = 20% using variable sensors based on $Ti_3C_2T_x$ nanosheets, KWO nanorods, KWO/Ti_3C_2Tx (1:2), KWO/$Ti_3C_2T_x$ (2:1), KWO/$Ti_3C_2T_x$ (1:1), KWO/$Ti_3C_2T_x$ (1:5), KWO/$Ti_3C_2T_x$ (4:1), and KWO/$Ti_3C_2T_x$ (9:1).

To evaluate the tolerance of humidity, the KWO/$Ti_3C_2T_x$ (2:1) nanocomposite-based sensor has been tested under different level of relative humidity (RH) at the room temperature. The result is shown in Figure 5. The nanocomposite, KWO/$Ti_3C_2T_x$ (2:1) nanocomposite shows relative stable baseline resistance (red color) while RH is from 10% up to 86%. Considering the less influence of RH but much higher sensitivity to acetone, KWO/$Ti_3C_2T_x$ (2:1) nanocomposite shows the best sensing response to acetone at room temperature. The selectivity of KWO/$Ti_3C_2T_x$ (2:1) nanocomposite-based sensor can be evaluated via referring to the selectivity of KWO-based sensors, which has been studied in other work [24].

The potential sensing mechanism of KWO/$Ti_3C_2T_x$ nanocomposite (2:1) to detect acetone, can be explained: (1) 1D KWO nanorods is a *p*-type semiconductor [22]. Although the nanocomposite has changed the crystal structure of the material, the Hall Effect measurement reveals that KWO/$Ti_3C_2T_x$ nanocomposites still are *p*-type semiconducting properties. The XRD spectra further clearly show that the content of $Ti_3C_2T_x$ is much lower comparing to the content of KWO in nanocomposites. Therefore, the property of material semiconducting in nanocomposites has no change. This means the majority carriers in nanocomposites are still holes. Once electron rich compounds, such as acetone, absorb onto KWO/$Ti_3C_2T_x$, acetone molecules will donate electrons and then combine with holes to result in the increase of resistance of the sensing materials. (2) The KWO room-temperature ferroelectric property is still the major reason to cause an effective charge transfer between KWO and acetone and realize selective detection of acetone [22,27–29]. (3) The high electrical conductivity of $Ti_3C_2T_x$ MXene and the interfacial interaction between $Ti_3C_2T_x$and KWO not only can lower the signal noise, but also can further enhance the charge transfer within the material. In other words, $Ti_3C_2T_x$ MXenes have been used as an efficient charge transfer material for biosensors. Herein, it is believed they play a similar role in the KWO/$Ti_3C_2T_x$ material sensing acetone. While they likely do not contribute much to the interaction with acetone, the $Ti_3C_2T_x$ MXenes help to lower the baseline resistance of the sensor film and provide a much higher signal to noise ratio. In other words, the $Ti_3C_2T_x$ MXene works as a type of electron collector which can help KWO more efficiently transfer charges while interacting with acetone.

More study into the mechanism at contact between the two materials should be studied in order to fortify this theory.

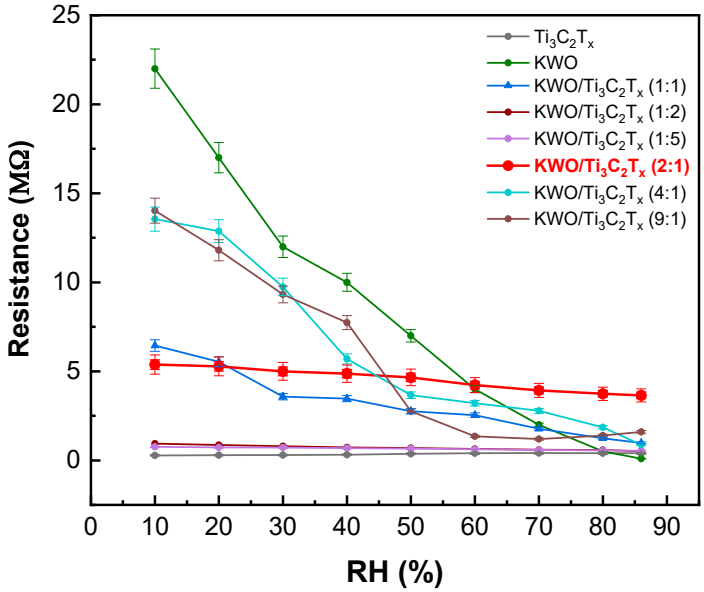

Figure 5. Resistance and RH relationship based on variable nanomaterials: $Ti_3C_2T_x$ nanosheets, KWO nanorods, KWO/$Ti_3C_2T_x$ (1:2), KWO/$Ti_3C_2T_x$ (2:1), KWO/$Ti_3C_2T_x$ (1:1), KWO/$Ti_3C_2T_x$ (1:5), KWO/$Ti_3C_2T_x$ (4:1), and KWO/$Ti_3C_2T_x$ (9:1).

In a word, the KWO/$Ti_3C_2T_x$ (2:1) nanocomposite is a new functionalized sensing material with great potential for application in the breath acetone sensor device. This device can deliver a low-cost, non-invasive, high accuracy, and portable device, with less interference of humidity, for early and rapid diabetes detection and long-term health monitoring with extreme high signal-to-noise ratio (SNR).

4. Conclusions

In summary, a new functionalized nanocomposite made by 1D nanorods, KWO, and 2D nanosheets, $Ti_3C_2T_x$ nanosheets, with ratio of 2:1, has been synthesized and used to detect acetone, the breath biomarker of diabetes. The experimental results exhibit significant improvement of sensing response of KWO/$Ti_3C_2T_x$ (2:1) nanocomposite to acetone. The sensitivity to detect acetone at room temperature is almost 10 times higher than the sensitivity of as-reported nanostructured KWO. In particular, the new nanocomposite, 1D/2D KWO/$Ti_3C_2T_x$ shows much less interference with humidity with extreme high signal-to-noise ratio (SNR) and capability of miniaturization and integration. A proposed sensing mechanism based on the *p*-type semiconducting property, ferroelectricity, extremely large surface, and much better conductivity has been discussed. Although more systematic understanding of the sensing mechanism is still under investigation, the initial study indicates KWO/$Ti_3C_2T_x$ (2:1) nanocomposite is a very promising new sensing material for application in acetone detection and diabetes care.

Author Contributions: O.A. initially wrote the paper and conducted experiments; M.S. worked on the major revision and paper submission. M.J. preformed all XRD, FT-IR, and Raman spectroscopy experiments, analyzed data, and synthesized the materials; Q.Z. designed material synthesis procedures and analyzed experimental data; D.W. wrote and finalized the paper, performed sensing experiments, analyzed experimental data, and led the research team. All authors have read and agreed to the published version of the manuscript.

Funding: This work is supported in part by the Offerdahl Seed Grant, NDSU Centennial Endowment Award, FAR0029296; and ND NASA EPSCoR research grant, FAR0030154, and ND EPSCoR seed award, FAR0030452.

Acknowledgments: We wish to acknowledge the NDSU Core Research Facilities for providing access to microfabrication tools and materials characterization instruments.

Conflicts of Interest: The authors declare no conflict of interest.

References

1. International Diabetes Federation (IDF). *Diabetes Atlas*; Hoorens Printing NV: Brussels, Belgium, 2006.
2. Saasa, V.; Beukes, M.; Lemmer, Y.; Mwakikunga, B. Blood Ketone Bodies and Breath Acetone Analysis and Their Correlations in Type 2 Diabetes Mellitus. *Diagnostics* **2019**, *9*, 224. [CrossRef] [PubMed]
3. Wilson, A.D. Application of electronic-nose technologies and VOC-biomarkers for the noninvasive early diagnosis of gastrointestinal diseases. *Sensors* **2018**, *18*, 2613. [CrossRef] [PubMed]
4. Ruzsanyi, V.; Kalapos, M.P. Breath acetone as a potential marker in clinical practice. *J. Breath Res.* **2017**, *11*, 024002. [CrossRef] [PubMed]
5. Rydosz, A. A negative correlation between blood glucose and acetone measured in healthy and type 1 diabetes mellitus patient breath. *J. Diabetes Sci. Technol.* **2015**, *9*, 881–884. [CrossRef] [PubMed]
6. Sun, M.; Zhao, X.; Yin, H.; Wang, Z.; Jiang, C.; Liu, W.; Chen, Z.; Yuan, Y.; Li, Y.; Wang, C. Study of breath acetone and its correlations with blood glucose and blood beta-hydroxybutyrate using an animal model with lab-developed type 1 diabetic rats. *RSC Adv.* **2015**, *5*, 71002–71010. [CrossRef]
7. Galassetti, P.R.; Novak, B.; Nemet, D.; Rose-Gottron, C.; Cooper, D.M.; Meinardi, S.; Newcomb, R.; Zaldivar, F.; Blake, D.R. Breath ethanol and acetone as indicators of serum glucose levels: An initial report. *Diabetes Technol. Ther.* **2005**, *7*, 115–123. [CrossRef] [PubMed]
8. Phillips, M.; Greenberg, J. Ion-trap detection of volatile organic compounds in alveolar breath. *Clin. Chem.* **1992**, *38*, 60–65. [CrossRef]
9. Trotter, M.D.; Sulway, M.J.; Trotter, E. The rapid determination of acetone in breath and plasma. *Clin. Chim. Acta* **1971**, *35*, 137–143. [CrossRef]
10. Ueta, I.; Saito, Y.; Hosoe, M.; Okamoto, M.; Ohkita, H.; Shirai, S.; Tamura, H.; Jinno, K. Breath acetone analysis with miniaturized sample preparation device: In-needle preconcentration and subsequent determination by gas chromatography–mass spectroscopy. *J. Chromatogr. B* **2009**, *877*, 2551–2556. [CrossRef]
11. Lehnert, A.S.; Behrendt, T.; Ruecker, A.; Pohnert, G.; Trumbore, S.E. SIFT-MS optimization for atmospheric trace gas measurements at varying humidity. *Atmos. Meas. Tech.* **2020**, *13*, 3507–3520. [CrossRef]
12. Usman, F.; Dennis, J.O.; Ahmed, A.Y.; Meriaudeau, F.; Ayodele, O.B.; Rabih, A.A. A review of biosensors for non-invasive diabetes monitoring and screening in human exhaled breath. *IEEE Access* **2018**, *7*, 5963–5974. [CrossRef]
13. Lee, J.E.; Lim, C.K.; Park, H.J.; Song, H.; Choi, S.Y.; Lee, D.S. ZnO–CuO Core-Hollow Cube Nanostructures for Highly Sensitive Acetone Gas Sensors at the ppb Level. *ACS Appl. Mater. Interfaces* **2020**, *12*, 35688–35697. [CrossRef] [PubMed]
14. Kao, K.W.; Hsu, M.C.; Chang, Y.H.; Gwo, S.; Yeh, J.A. A sub-ppm acetone gas sensor for diabetes detection using 10 nm thick ultrathin InN FETs. *Sensors* **2012**, *12*, 7157–7168. [CrossRef] [PubMed]
15. Das, S.; Ghosh, S.; Kumar, R.; Bag, A.; Biswas, D. Highly sensitive acetone sensor based on Pd/AlGaN/GaN resistive device grown by plasma-assisted molecular beam epitaxy. *IEEE Trans. Electron Devices* **2017**, *64*, 4650–4656. [CrossRef]
16. Qiu, Z.; Hua, Z.; Li, Y.; Wang, M.; Huang, D.; Tian, C.; Zhang, C.; Tian, X.; Li, E. Acetone sensing properties and mechanism of Rh-Loaded WO_3 nanosheets. *Front. Chem.* **2018**, *6*, 385. [CrossRef]
17. Kim, N.H.; Choi, S.J.; Yang, D.J.; Bae, J.; Park, J.; Kim, I.D. Highly sensitive and selective hydrogen sulfide and toluene sensors using Pd functionalized WO_3 nanofibers for potential diagnosis of halitosis and lung cancer. *Sens. Actuators B* **2014**, *193*, 574–581. [CrossRef]
18. Tomer, V.K.; Singh, K.; Kaur, H.; Shorie, M.; Sabherwal, P. Rapid acetone detection using indium loaded WO3/SnO2 nanohybrid sensor. *Sens. Actuators B* **2017**, *253*, 703–713. [CrossRef]
19. Khokhra, R.; Bharti, B.; Lee, H.N.; Kumar, R. Visible and UV photo-detection in ZnO nanostructured thin films via simple tuning of solution method. *Sci. Rep.* **2017**, *7*, 15032. [CrossRef]
20. Wang, X.; Qin, H.; Pei, J.; Chen, Y.; Li, L.; Xie, J.; Hu, J. Sensing performances to low concentration acetone for palladium doped $LaFeO_3$ sensors. *J. Rare Earths* **2016**, *34*, 704–710. [CrossRef]
21. Wang, F.; Yang, C.; Duan, M.; Tang, Y.; Zhu, J. TiO2 nanoparticle modified organ-like Ti_3C_2 MXene nanocomposite encapsulating hemoglobin for a mediator-free biosensor with excellent performances. *Biosens. Bioelectron.* **2015**, *74*, 1022–1028. [CrossRef]
22. Zhang, Q.; Wang, D. Room temperature acetone sensor based on nanostructured $K_2W_7O_{22}$. In Proceedings of the IEEE SENSORS 2016, Orlando, FL, USA, 30 October–3 November 2016; pp. 1–3. [CrossRef]

23. Barsan, N.; Weimar, U. Fundamentals of Metal Oxide Gas Sensors. In Proceedings of the 14th International Meeting on Chemical Sensors-IMCS 2012, Nuremberg, Germany, 20–23 May 2012; pp. 618–621.
24. Varghese, O.K.; Grimes, C.A. Metal oxide nanoarchitectures for environmental sensing. *J. Nanosci. Nanotechnol.* **2003**, *3*, 277–293. [CrossRef] [PubMed]
25. Wang, D.; Zhang, Q.; Hossain, M.R.; Johnson, M. High sensitive breath sensor based on nanostructured $K_2W_7O_{22}$ for detection of type 1 diabetes. *IEEE Sens. J.* **2018**, *18*, 4399–4404. [CrossRef]
26. Hossain, M.R.; Zhang, Q.; Johnson, M.; Wang, D. Highly Sensitive Room-Temperature Sensor Based on Nanostructured $K_2W_7O_{22}$ for Application in the Non-Invasive Diagnosis of Diabetes. *Sensors* **2018**, *18*, 3703. [CrossRef]
27. Johnson, M.E.; Zhang, Q. K_xWO Is a Novel Ferroelectric Nanomaterial for Application as a Room Temperature Acetone Sensor. *Nanomaterials* **2020**, *10*, 225. [CrossRef] [PubMed]
28. Johnson, M.; Zhang, Q.; Wang, D. Room-temperature ferroelectric $K_2W_7O_{22}$ (KWO) nanorods as a sensor material for the detection of acetone. *Med. Devices Sens.* **2019**, *2*, e10044. [CrossRef]
29. Hossain, M.R.; Zhang, Q.F.; Johnson, M.; Ama, O.; Wang, D.L. Investigation of Different Materials as Acetone Sensors for Application in Type-1 Diabetes Diagnosis. *Biomed. J. Sci. Tech. Res.* **2019**, *14*, 10940–10945.
30. Hossain, M.R.; Zhang, Q.; Johnson, M.; Wang, D. Investigation of humidity cross-interference effect on acetone breath sensor based on nanostructured $K_2W_7O_{22}$. *Eng. Press* **2017**, *1*, 30–34.
31. Lukatskaya, M.R.; Mashtalir, O.; Ren, C.E.; Dall'Agnese, Y.; Rozier, P.; Taberna, P.L.; Naguib, M.; Simon, P.; Barsoum, M.W.; Gogotsi, Y. Cation intercalation and high volumetric capacitance of two-dimensional titanium carbide. *Science* **2013**, *341*, 1502–1505. [CrossRef] [PubMed]
32. Ghidiu, M.; Lukatskaya, M.R.; Zhao, M.Q.; Gogotsi, Y.; Barsoum, M.W. Conductive two-dimensional titanium carbide 'clay' with high volumetric capacitance. *Nature* **2014**, *516*, 78–81. [CrossRef]
33. Anasori, B.; Lukatskaya, M.R.; Gogotsi, Y. 2D metal carbides and nitrides (MXenes) for energy storage. *Nat. Rev. Mater.* **2017**, *2*, 16098. [CrossRef]
34. Huang, K.; Li, Z.; Lin, J.; Han, G.; Huang, P. Two-dimensional transition metal carbides and nitrides (MXenes) for biomedical applications. *Chem. Soc. Rev.* **2018**, *47*, 5109–5124. [CrossRef] [PubMed]
35. Khazaei, M.; Arai, M.; Sasaki, T.; Ranjbar, A.; Liang, Y.; Yunoki, S. OH-terminated two-dimensional transition metal carbides and nitrides as ultralow work function materials. *Phys. Rev. B* **2015**, *92*, 075411. [CrossRef]
36. Yuan, W.; Yang, K.; Peng, H.; Li, F.; Yin, F. A flexible VOCs sensor based on a 3D Mxene framework with a high sensing performance. *J. Mater. Chem. A* **2018**, *6*, 18116–18124. [CrossRef]
37. Allah, A.E.; Wang, J.; Kaneti, Y.V.; Li, T.; Farghali, A.A.; Khedr, M.H.; Nanjundan, A.K.; Ding, B.; Dou, H.; Zhang, X.; et al. Auto-programmed heteroarchitecturing: Self-assembling ordered mesoporous carbon between two-dimensional $Ti_3C_2T_x$ MXene layers. *Nano Energy* **2019**, *65*, 103991. [CrossRef]
38. Johnson, M.; Zhang, Q.; Wang, D. Titanium carbide MXene: Synthesis, electrical and optical properties and their applications in sensors and energy storage devices. *Nanomater. Nanotechnol.* **2019**, *9*, 1–9. [CrossRef]
39. Alhabeb, M.; Maleski, K.; Anasori, B.; Lelyukh, P.; Clark, L.; Sin, S.; Gogotsi, Y. Guidelines for synthesis and processing of two-dimensional titanium carbide ($Ti_3C_2T_x$ MXene). *Chem. Mater.* **2017**, *29*, 7633–7644. [CrossRef]
40. Michael, J.; Wang, D.L.; Zhang, Q.F. Synthesis of high yield, pure Ti_3C_2 MXene using high temperature etching. *Nanomaterials* **2020**, in press.
41. Cao, M.; Wang, F.; Wang, L.; Wu, W.; Lv, W.; Zhu, J. Room temperature oxidation of Ti_3C_2 MXene for supercapacitor electrodes. *J. Electrochem. Soc.* **2017**, *164*, A3933. [CrossRef]
42. Kim, S.J.; Koh, H.J.; Ren, C.E.; Kwon, O.; Maleski, K.; Cho, S.Y.; Anasori, B.; Kim, C.K.; Choi, Y.K.; Kim, J.; et al. Metallic $Ti_3C_2T_x$ MXene Gas Sensors with Ultrahigh Signal-to-Noise Ratio. *ACS Nano* **2018**, *12*, 986–993. [CrossRef]